ACTA ACUSTICA UNITED WITH ACUSTICA
Vol. 90 (2004) 819 – 829

The Interaction of Inhomogeneous Waves and Gaussian Beams with Mud in Between a Hard Solid and an Ideal Liquid

Nico F. Declercq*, Oswald Leroy**, Joris Degrieck*, Jeroen Vandeputte**

*: Soete Laboratory, Department of Mechanical Construction and Production, Faculty of Engineering, Ghent University, Sint Pietersnieuwstraat 41, 9000 Gent, Belgium. NicoF.Declercq@UGent.be

**: Interdisciplinary Research Center, KULeuven Campus Kortrijk, E. Sabbelaan 53, 8500 Kortrijk, Belgium.

Summary
Mud is classified as a Bingham liquid, which, situated in between a hard solid and an ideal liquid, forms a rheological system in which the physical parameters vary continuously. Moreover, inside this liquid, there is often a transition zone (at the nautical bottom) in which the shear wave velocity varies almost exponentially. First we translate this rheological system into a theoretical rheological model that is numerically susceptible to predict its physical influence on impinging sound. Then, we show theoretically how the interaction of sound with this rheological model is solved. Finally, we present some numerical results for impinging inhomogeneous waves and we show how a bounded beam interacts with this continuously layered system. The paper shows that it is theoretically possible to apply the inhomogeneous wave theory for such a system and also that the Fourier description of bounded beams works excellent for describing the propagation of bounded beams through mud. Even though it is widely known that echo sounding cannot reveal the position of the nautical bottom, we show that its position influences the reflected beam pattern for oblique incidence, which is promising for nautical depth determination in harbors and rivers.

PACS no. 43.20.Bi, 43.20.El

1. Introduction

It is known from various textbooks that a Bingham liquid is a liquid that behaves like solid under static conditions, but starts to flow if a yield force is applied that exceeds a critical value. This phenomenon is often called plastic flow. The description of this flow is beyond our intentions and is left as a matter of investigation for rheologists. Bingham liquids also have other properties that are more interesting at this point. We are primarily interested in the consequences of a Bingham liquid at rest, i.e. under macroscopic static conditions, on traversing sound. An important feature of liquids, showing Bingham behavior, at rest, is the appearance of a spatial phase transition zone below which the liquid can be fully described as a Bingham liquid and above which the liquid behaves almost as if it were an ideal liquid. Such liquids appear in many branches of science and everyday life materials such as fresh concrete [1, 2], lava [3, 4], mud [5, 6, 7, 8], molten plastic and even ketchup. The range of applications where Bingham like behaving liquids appear is even wider. They appear in the study of periodical river floods [9], gravity driven floods [10], sediment mobility [11], climate evolution [12], archeology [13, 14, 15], meteorology [16], geology [17], emulsion [18], and even in engineering problems when bridges are to be built [19] or in the oil industry and ecology [20].

Especially in the shipping and dredging industry, it is of primordial importance to know the nautical depth in rivers and harbors. The nautical depth is determined by mud characteristics at the bottom of waterways, see Figure 1. It forms the transition between navigable mud and non-navigable mud. Navigable mud is almost like water, whereas non-navigable mud is almost like clay.

In many of the mentioned fields and especially for monitoring waterways, the use of ultrasound is already generally adopted in its simplest form such as echo sounding [21, 22, 23], where it is highly competitive with other techniques such as laser bathymetry [24]. Nevertheless, the problem with echo sounding is the fact that the nautical bottom cannot be detected when normal incidence is applied. The reason is that this transition zone consists of an almost abrupt change in shear sound parameters, but not in longitudinal sound parameters. Since normal incident sound doesn't stimulate shear waves, it is not susceptible for the transition zone. Echo sounding is hence only practicable for determination of the depth where the

Received 16 October 2003,
accepted 25 May 2004.

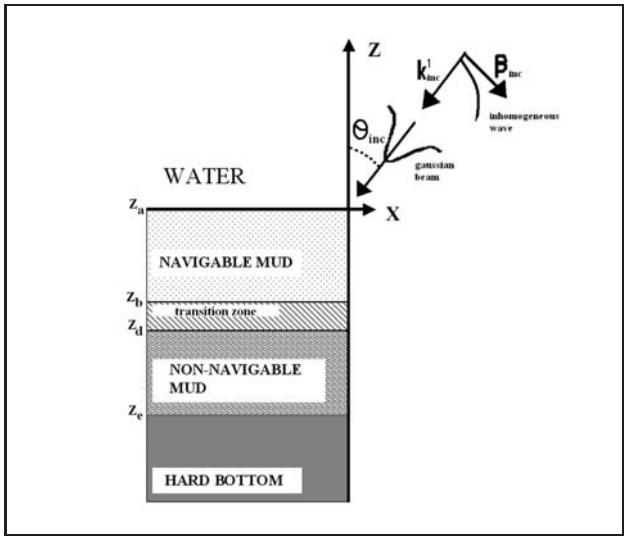

Figure 1. A schematic of the different layers in a system of mud in between a hard solid and an ideal liquid.

hard bottom starts (sand, rocks, concrete, ...) and where the transition between water and navigable mud occurs, not for determining the nautical depth, which is always located somewhere in between. It is therefore interesting to develop a theoretical model that describes a more advanced interaction of sound with liquids showing Bingham behavior. More particularly, understanding of the interaction with inhomogeneous waves and obliquely incident bounded beams might be a stimulus to create more sophisticated technologies to detect the transition zone.

In what follows, we study a rheological system which is quite similar to mud in a harbor. The parameters used in the numerical examples for describing mud do not perfectly correspond with the exact parameters, but they are realistic. For simplicity we have neglected damping in the numerical examples, except for the hard bottom. Nevertheless, because damping plays an important role in real physical mud, we have incorporated damping in the theoretical description.

2. Theoretical description of the rheological model

2.1. Bulk properties

The different layers that are mentioned below, are depicted in Figure 1. For reasons of simplicity, we limit our model to where the rheological system of interest is for our purpose fully characterized by its dimensions and its density and sound velocity. The latter two are supposed to vary continuously with depth. The influence of the specific microscopic structure on what we are interested in, is hence considered to be fully contained in the density and velocity values. Therefore, we do not consider explicitly the occurrence of air bubbles [25, 26] or the presence of grains [27]. The latter assumption is justified by the known fact that liquids showing Bingham behavior, like for example mud, cannot be reduced to special cases of grainy solids like sand [28].

The rheological system consists of a layer of liquid showing Bingham behavior (for brevity called 'Bingham layer'), covered with water and resting on an infinitely thick layer of material with constant bulk properties ('the underground or the hard bottom'). The Bingham layer itself is built up by three interlayers. The upper interlayer is that where the liquid finds itself under such physical conditions that it is almost an ideal fluid (e.g. navigable mud). The lower interlayer is that where the liquid has been transformed into a Bingham liquid (e.g. non-navigable mud). The middle layer is the so called 'transition zone'.

Moreover, the upper interlayer, respectively the lower interlayer, has low respectively high constant shear velocity, while the transition zone has a nonlinearly continuously varying shear velocity, connecting that of the upper interlayer to that of the lower interlayer. It is in this layer that the so called 'phase transition' appears. We always consider the density varying linearly throughout the system. The dilatational velocity is considered to be quasi linearly varying with depth, i.e. linearly if we only take a look at the particular points mathematically separating each layer. Demanding pure linearity would be too rigorous, leading to inconsistency of the physical parameters.

If the density and the sound velocities vary sufficiently slow with depth within each layer, then, locally, plane waves as well as inhomogeneous waves will be solutions of the wave equation. Under these circumstances, it has been shown by Brekhovskikh and Godin [29] that if φ is the longitudinal wave potential and ψ the shear wave potential, then, omitting the time dependence $\exp(-\mathrm{i}\omega t)$

$$\varphi(x,z) \;=\; \Phi(z)\exp\left(\mathrm{i}k_{d,x}x\right), \tag{1}$$

$$\boldsymbol{\psi}(x,z) \;=\; \psi(x,z)\boldsymbol{e}_y = \Psi(z)\exp\left(\mathrm{i}k_{s,x}x\right)\boldsymbol{e}_y, \tag{2}$$

with

$$\frac{\partial^2\Phi(z)}{\partial z^2} + g_d(z)\Phi(z) = 0, \tag{3}$$

$$\frac{\partial^2\Psi(z)}{\partial z^2} + g_s(z)\Psi(z) = 0. \tag{4}$$

Since inhomogeneous waves are local solutions of the wave equation, the dispersion relation for inhomogeneous waves [30] holds locally and we get

$$g_d(z) + k_{d,x}^2 \;=\; \frac{\omega^2}{\left(v_d^p(z)\right)^2} - \left(\alpha_{d,0}^p(z)\right)^2 = \frac{\omega^2\rho(z)}{\lambda(z)+2\mu(z)}, \tag{5}$$

$$g_s(z) + k_{s,x}^2 \;=\; \frac{\omega^2}{\left(v_s^p(z)\right)^2} - \left(\alpha_{s,0}^p(z)\right)^2 = \frac{\omega^2\rho(z)}{\mu(z)}. \tag{6}$$

The system is considered to behave viscoelastic, whence [31, 32, 33, 34, 35] for each spot in layer 'p'

$$\lambda^p(z) \;=\; \lambda_1^p(z) - \mathrm{i}\omega\lambda_2^p(z), \tag{7}$$

$$\mu^p(z) = \mu_1^p(z) - \mathrm{i}\omega\mu_2^p(z), \tag{8}$$

with the Lamé constants λ_1^p and μ_1^p and viscoelastic constants λ_2^p and μ_2^p of (7)–(8) related to the intrinsic damping coefficient for shear waves $\alpha_{s,0}^p$, the shear wave velocity v_s^p, the intrinsic damping coefficient for longitudinal waves $\alpha_{d,0}^p$ and the longitudinal wave velocity v_d^p, through the dispersion relations [30] (5)–(6), giving

$$\mu_1^p = \omega^2\left(v_s^p\right)^2\rho^p\left(\omega - \alpha_{s,0}^p v_s^p\right)\frac{\alpha_{s,0}^p v_s^p + \omega}{\left(\omega^2 + (\alpha_{s,0}^p v_s^p)^2\right)^2}, \tag{9}$$

$$\mu_2^p = 2\alpha_{s,0}^p\omega^2\left(v_s^p\right)^3\frac{\rho^p}{\left(\omega^2 + (\alpha_{s,0}^p v_s^p)^2\right)^2}, \tag{10}$$

$$\lambda_2^p = 2\alpha_{d,0}^p\omega^2\left(v_d^p\right)^3\frac{\rho^p}{\left(\omega^2 + (\alpha_{d,0}^p v_d^p)^2\right)^2} - 2\mu_2^p, \tag{11}$$

$$\lambda_1^p = \omega^2\left(v_d^p\right)^2\rho^p\left(\omega - \alpha_{d,0}^p v_d^p\right)\frac{\alpha_{d,0}^p v_d^p + \omega}{\left(\omega^2 + (\alpha_{d,0}^p v_d^p)^2\right)^2} - 2\mu_1^p. \tag{12}$$

Whenever necessary, the longitudinal wave velocity v_d^p and the shear wave velocity v_s^p can be extracted from (9)–(12) and written as a function of the Lamé coefficients and the frequency. For brevity, in the sequel, we write

$$\lambda_3^p = -\mathrm{i}\omega\lambda_2^p, \tag{13}$$

$$\mu_3^p = -\mathrm{i}\omega\mu_2^p. \tag{14}$$

Relations (9)–(12) and the straightforward extraction of v_d^p and v_s^p are reported here for the first time. Before, solely approximations were published for extremely low damping coefficients [36, 37, 38].

The differential equations (3)–(4) can only be solved if g_q ($q = d, s$) are sufficiently 'uncomplicated' [29]. We limit the level of difficulty to g_q being constant or a linear function of z. Before describing the interaction of sound with the rheological system (see next paragraph), it is necessary to determine g_q for each layer. Taking into account the above stated properties of the sound velocities as a function of depth, we find for the intervals defined in Figure 1,

$g_s(z)$	$g_d(z)$
$z_a \to z_b$:	
$g_{s,ab}(z) = \tilde{k}_{s,ab}$	$g_{d,ab}(z) = \tilde{k}_{d,ab} + \tilde{p}_{d,ab}z$
$z_b \to z_d$:	
$g_{s,bd}(z) = \tilde{k}_{s,bd} + \tilde{p}_{s,bd}z$	$g_{d,bd}(z) = \tilde{k}_{d,bd} + \tilde{p}_{d,bd}z$
$z_d \to z_e$:	
$g_{s,de}(z) = \tilde{k}_{s,de}$	$g_{d,de}(z) = \tilde{k}_{d,de} + \tilde{p}_{d,de}z$

(15)

where each $\tilde{k}$ and $\tilde{p}$ have to be determined, so that the rheological system is consistent with (9)–(12) and the above stated properties of the density and sound velocities as a function of depth. The 'tilde' is there in order not to mix up with classical wave numbers. In what follows in this paragraph, all parameters describe the upper interlayer, the transition layer and the lower interlayer and not the covering ideal liquid or the solid underground. Therefore, for example a parameter ζ_e is the value of ζ at the spot $\lim_{\substack{z\to z_e\\ z<z_e}}(z)$.

The Lamé constants in the layers $[z_a, z_b]$, $[z_b, z_d]$ and $[z_d, z_e]$ are assumed to be continuous through their respective interfaces, whereas for μ_a, λ_a, ρ_a, μ_e, λ_e and ρ_e given edge parameters, we demand the following boundary conditions:

2.1.1. Boundary Conditions for Shear Parameters

We demand that for each $z \in [z_a, z_b]$

$$\frac{\mu_{ab}(z)}{\rho_{ab}(z)} = \frac{\mu_a}{\rho_a}, \tag{16}$$

and that for each $z \in [z_d, z_e]$

$$\frac{\mu_{de}(z)}{\rho_{de}(z)} = \frac{\mu_e}{\rho_e}, \tag{17}$$

which involves a constant shear velocity in the intervals $[z_a, z_b]$ and $z \in [z_d, z_e]$.

2.1.2. Boundary Conditions for Longitudinal Parameters

$$\lambda_{ab}(z_a) = \lambda_a, \tag{18}$$

$$\lambda_{de}(z_e) = \lambda_e. \tag{19}$$

2.1.3. Quasi Linearity of the Complex Longitudinal Velocity

Quasi linearity means linear if only the mathematical spots z_a, z_b, z_d and z_e are considered. The complex longitudinal velocity in a layer 'p', of which the real part is the genuine longitudinal wave velocity is defined as:

$$v_d^p = \sqrt{\frac{\lambda^p + 2\mu^p}{\rho^p}}. \tag{20}$$

Remark that this is consistent with (5), because it is the expression of the generalized complex wave velocity and not the real wave velocity.

2.1.4. Set of Equations of Boundary and Continuity Conditions

In what follows, we denote $\mu_{gn} = \mu_g(z_n)$.

Conditions (16)–(20) ultimately give:

$$\tilde{k}_{s,ab} = \frac{\rho_a\omega^2 - (\mu_{1a} + \mu_{3a})(k_{s,x})^2}{\mu_{1a} + \mu_{3a}}, \tag{21}$$

$$\tilde{k}_{s,de} = \frac{\rho_e\omega^2 - (\mu_{1e} + \mu_{3e})(k_{s,x})^2}{\mu_{1e} + \mu_{3e}}, \tag{22}$$

$$\begin{pmatrix} -1 & -z_b \\ 1 & z_d \end{pmatrix}\begin{pmatrix} \tilde{k}_{s,bd} \\ \tilde{p}_{s,bd} \end{pmatrix} = \begin{pmatrix} -\tilde{k}_{s,ab} \\ \tilde{k}_{s,de} \end{pmatrix}, \tag{23}$$

and

$$\begin{pmatrix} 0 & 0 & 1 & z_d & 0 & 0 \\ 1 & z_b & 0 & 0 & 0 & 0 \\ 0 & 0 & 0 & 0 & 1 & z_e \\ 0 & 0 & 1 & z_d & -1 & -z_d \\ 1 & z_b & -1 & -z_d & 0 & 0 \\ 1 & z_a & 0 & 0 & 0 & 0 \end{pmatrix} \begin{pmatrix} \tilde{k}_{d,ab} \\ \tilde{p}_{d,ab} \\ \tilde{k}_{d,bd} \\ \tilde{p}_{d,bd} \\ \tilde{k}_{d,de} \\ \tilde{p}_{d,de} \end{pmatrix} = \begin{pmatrix} \omega^2 \Big[\sqrt{\frac{\lambda_{ab}(z_a)+2\mu_{ab}(z_a)}{\rho_{ab}(z_a)}} \frac{z_e - z_d}{z_e - z_a} \\ \quad + \sqrt{\frac{\lambda_{de}(z_e)+2\mu_{de}(z_e)}{\rho_{de}(z_e)}} \frac{z_d - z_a}{z_e - z_a} \Big]^{-2} - (k_{d,x})^2 \\ \omega^2 \Big[\sqrt{\frac{\lambda_{ab}(z_a)+2\mu_{ab}(z_a)}{\rho_{ab}(z_a)}} \frac{z_e - z_b}{z_e - z_a} \\ \quad + \sqrt{\frac{\lambda_{de}(z_e)+2\mu_{de}(z_e)}{\rho_{de}(z_e)}} \frac{z_b - z_a}{z_e - z_a} \Big]^{-2} - (k_{d,x})^2 \\ \frac{\omega^2 \rho_e}{\lambda_e + 2\mu_{de}} - (k_{d,x})^2 \\ 0 \\ 0 \\ \frac{\omega^2 \rho_a}{\lambda_a + 2\mu_{ab}} - (k_{d,x})^2 \end{pmatrix} \quad (24)$$

Equations (21)–(24) enable us to determine the self consistent values $\tilde{k}_{s,ab}$, $\tilde{k}_{s,de}$, $\tilde{k}_{s,bd}$, $\tilde{p}_{s,bd}$, $\tilde{k}_{d,ab}$, $\tilde{p}_{d,ab}$, $\tilde{k}_{d,bd}$, $\tilde{p}_{d,bd}$, $\tilde{k}_{d,de}$, $\tilde{p}_{d,de}$ that determine the rheological system that is considered here. In Figure 2, an example is given as how the wave velocities and density may evolve as a function of depth. More details concerning Figure 2 will follow in the next paragraph.

3. The interaction of inhomogeneous waves with the rheological model

Before building a continuity matrix, it is first necessary to find solutions of (1)–(4).

If we rewrite equations (3)–(4) for $f = \Phi$ or $f = \Psi$ as

$$\frac{\partial^2 f}{\partial z^2} - \Big(-\tilde{p}z - \tilde{k} \Big) f = 0, \quad (25)$$

and take

$$\gamma = \big(-\tilde{p} \big)^{-2/3} \big(-\tilde{p}z - \tilde{k} \big) \quad (26)$$

then (25) becomes

$$\frac{\partial^2 f}{\partial \gamma^2} - \gamma f = 0, \quad (27)$$

which is the Airy equation, whence [39]

$$f = C_m \mathrm{Ary}_0(\gamma) + C_w \mathrm{Ary}_2(\gamma), \quad (28)$$

with

$$\frac{\partial f}{\partial z} = -\frac{\tilde{p}}{(-\tilde{p})^{2/3}} \big[C_m \mathrm{Ary}_1(\gamma) + C_w \mathrm{Ary}_3(\gamma) \big]. \quad (29)$$

The Airy function of the first kind is denoted by Ary_0 with derivative Ary_1, while the Airy function of the second kind is denoted by Ary_2 with derivative Ary_3.

In case $\tilde{p} = 0$,

$$f = C_m \exp\big(\mathrm{i}\sqrt{\tilde{k}z} \big) + C_w \exp\big(-\mathrm{i}\sqrt{\tilde{k}z} \big). \quad (30)$$

Taking into account relations (15), we use the following acoustical potentials ('inc'=incident, 'r'=reflected, 'u'=underground):

$$\Phi^{inc} = A \exp\big(\mathrm{i}k_{inc,z} z \big), \quad (31)$$

$$\Phi^{r} = Q \exp\big(-\mathrm{i}k_{inc,z}(z - z_a) \big), \quad (32)$$

$$\Psi_{ab}(z) = C_{ms,ab} \exp\big(\mathrm{i}\sqrt{\tilde{k}_{s,ab}}(z - z_a) \big) + C_{ws,ab} \exp\big(-\mathrm{i}\sqrt{\tilde{k}_{s,ab}}(z - z_b) \big), \quad (33)$$

$$\Phi_{ab}(z) = C_{md,ab}\mathrm{Ary}_0(\gamma_{d,ab}) + C_{wd,ab}\mathrm{Ary}_2(\gamma_{d,ab}), \quad (34)$$

$$\Psi_{bd}(z) = C_{ms,bd}\mathrm{Ary}_0(\gamma_{s,bd}) + C_{ws,bd}\mathrm{Ary}_2(\gamma_{s,bd}), \quad (35)$$

$$\Phi_{bd}(z) = C_{md,bd}\mathrm{Ary}_0(\gamma_{d,bd}) + C_{wd,bd}\mathrm{Ary}_2(\gamma_{d,bd}), \quad (36)$$

$$\Psi_{de}(z) = C_{ms,de} \exp\big(\mathrm{i}\sqrt{\tilde{k}_{s,de}}(z - z_d) \big) + C_{ws,de} \exp\big(-\mathrm{i}\sqrt{\tilde{k}_{s,de}}(z - z_e) \big), \quad (37)$$

$$\Phi_{de}(z) = C_{md,de}\mathrm{Ary}_0(\gamma_{d,de}) + C_{wd,de}\mathrm{Ary}_2(\gamma_{d,de}), \quad (38)$$

$$\Psi_{u}(z) = S \exp\big(\mathrm{i}k^s_{u,z}(z - z_e) \big), \quad (39)$$

$$\Phi_{u}(z) = D \exp\big(\mathrm{i}k^d_{u,z}(z - z_e) \big). \quad (40)$$

The unknown parameters Q, S, D and all Cs can now be obtained by creating a continuity matrix that connects the sound fields in each layer. The spots z_a and z_e involve abrupt changes of the sound velocity and density. Hence, we demand continuity of normal stress and displacement there. All other spots involve continuous changes of density and sound velocity, whence we demand continuity of the acoustical potentials (31)–(40) and their first derivatives.

The stress tensor is given by

$$\sigma_{ij} = \delta_{ij}\tilde{\lambda}\varepsilon_{kk} + 2\tilde{\mu}\varepsilon_{ij}, \quad (41)$$

where we have used the double suffix Einstein notation convention. The strain tensor ε is denoted by its elements

$$\varepsilon_{ij} = \frac{1}{2}\left[\frac{\partial u_i}{\partial r_j} + \frac{\partial u_j}{\partial r_i} \right], \quad (42)$$

with displacement vector

$$\boldsymbol{u} = \nabla\varphi + \nabla \times \Psi. \quad (43)$$

The continuity matrix can be found straightforwardly from the continuity conditions given above and taking into account Snell's law stating that the lateral component of the wave vector remains unaltered in the layered system. The result is:

$$\big[CONT\big]_{15\times 15}\big[U\big]_{15\times 1} = \big[K\big]_{15\times 1}, \quad (44)$$

with

$$U = [Q, C_{md,ab}, C_{wd,ab}, C_{ms,ab}, C_{ws,ab}, C_{md,bd}, C_{wd,bd}, C_{ms,bd}, C_{ws,bd}, C_{md,de},$$

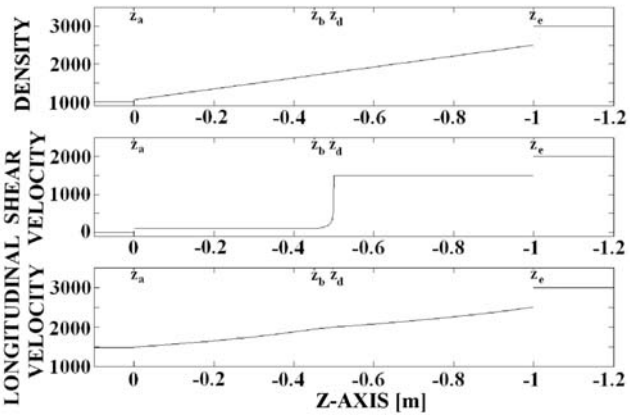

Figure 2. Density and sound velocities as a function of depth for the system shown in Figure 1 and applied in calculations that produce Figures 3–10.

$$C_{wd,de}, C_{ms,de}, C_{ws,de}, D, S\big]^T, \tag{45}$$

$$K = \big[-2\mu_w k_{inc,x} k_{inc,z} \Phi^{inc}, \mathrm{i} k_{inc,z} \Phi^{inc}, (-\omega^2 \rho_w + 2\mu_w k_{inc,x}^2)\Phi^{inc}, 0, \ldots, 0\big]^T, \tag{46}$$

and

$$CONT = \begin{bmatrix} c1 & 0 & 0 & 0 \\ c2 & c3 & 0 & 0 \\ 0 & c4 & c5 & 0 \\ 0 & 0 & c6 & c7 \end{bmatrix}, \tag{47}$$

with in $[CONT]$ blocks of zeros denoted by '0' and the other elements given in (A1)–(A7).

4. Numerical results for incident inhomogeneous waves

To keep things short, incident inhomogeneous waves are described as pure plane waves, except that their wave vector is complex valued. Hence

$$\boldsymbol{k}_{inc} = \boldsymbol{k}_{inc}^1 + \mathrm{i}\boldsymbol{k}_{inc}^2, \tag{48}$$

with

$$\boldsymbol{k}_{inc}^2 \text{"} = \boldsymbol{\alpha}_{inc} - \boldsymbol{\beta}_{inc}. \tag{49}$$

$\boldsymbol{\alpha}_{inc}$ is the damping vector, while $\boldsymbol{\beta}_{inc}$ is the inhomogeneity vector. More properties can be found in numerous articles [30, 40]. An example of the amplitude profile and wave vectors of an undamped inhomogeneous wave is shown in the right upper corner of Figure 1. It is known that if pure homogeneous plane waves, i.e. $\boldsymbol{k}_{inc}^2 = 0$, scatter from plane interfaces, that in general inhomogeneous waves will be transmitted into the opposing medium if damping is present. However, it has also been shown before that incident inhomogeneous waves can deliver some insight into what will happen to the profile of bounded beams if they are reflected from the interface [41]. The main problem however with the formation of bounded beams by a superposition of inhomogeneous waves is that,

Table I. Boundary values at some particular spots in the layered system. v_{long}: Longitudinal velocity.

Spot	Position [m]	Density [kg/m^3]	v_{long} [m/s]
z_0	0.1	-	-
z_a	0	1050	1490
z_b	-0.45	-	-
z_d	-0.50	-	-
z_e	-1	2500	2500

Table II. Boundary values in some particular intervals in the layered system. ρ: Density, v_{long}: Longitudinal velocity, v_{shear}: Shear velocity.

Interval	ρ [kg/m^3]	v_{long} [m/s]	v_{shear} [m/s]
$z_0 \to z_a$	1050	1480	0
$z_a \to z_b$	-	-	100
$z_d \to z_e$	-	-	1500
Underground (hard bottom)	3000	3000	2000

besides its great opportunities to describe and understand beam displacements like the Schoch effect, the propagation of such mathematical beams is often not very convenient. Since it is our aim to depict exactly how a transmitted bounded beam propagates into the layers, we choose not to decompose bounded beams into inhomogeneous waves, but into pure plane waves using the Fourier decomposition.

Nevertheless, a limited study of the reflection coefficient of inhomogeneous waves gives us the opportunity to already predict some phenomena that will occur in the next paragraph, where the reflection and transmission of bounded beams are studied. As an example, we have taken the parameters of Tables I and II, which are graphically given in Figure 2. Furthermore, we have solely considered (strong) damping in the underground, not in the other layers. In Figure 3, a frequency of 150 kHz is applied. It is seen that the reflection coefficient (shown as its intensity in dB) as a function of the angle of incidence (defined in Figure 1) and as a function of the incident inhomogeneity (a positive inhomogeneity β_{inc} is also shown in Figure 1), shows an elevated intensity (peaks) in some regions and much smaller intensity in other regions. This phenomenon also appears if the interaction of inhomogeneous waves with metal plates is considered. It is well known that a reflection coefficient less than unity shifts an inhomogeneous wave to the direction in which it shows exponential growth, while a reflection coefficient exceeding unity shifts an inhomogeneous wave to direction in which it shows exponential decay. Furthermore, the smaller the value of $|\beta_{inc}|$, the larger the shift to left or right. Because the reflection coefficients for positive inhomogeneities is nowhere negative (in dB), it can already be concluded that inhomogeneous waves will never be shifted in the positive x-direction. Hence, a backward beam shift will never oc-

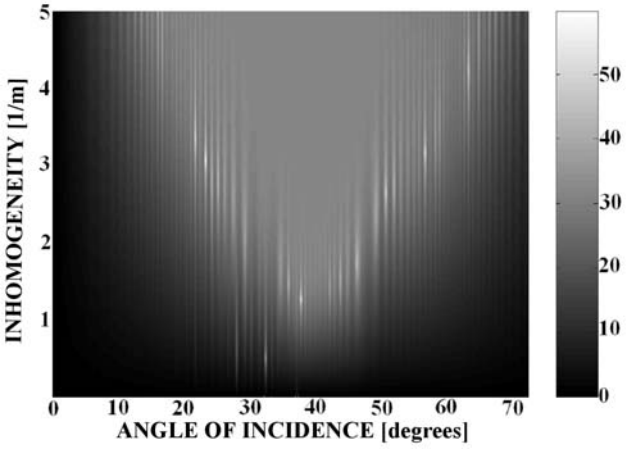

Figure 3. Intensity in dB of reflected inhomogeneous waves as a function of the angle of incidence and inhomogeneity.

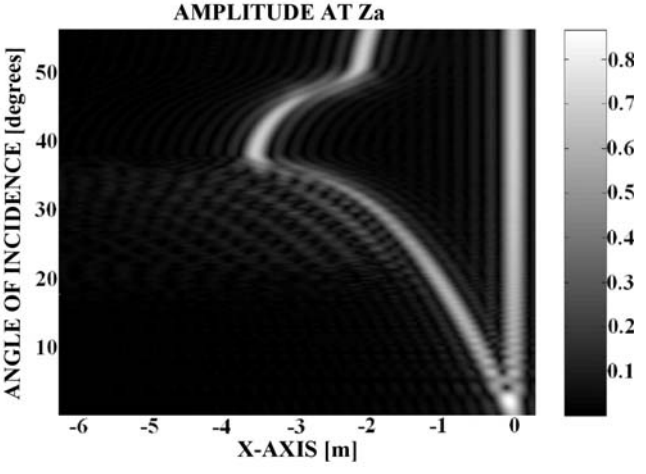

Figure 4. Total amplitude at $z = z_a$ as a function of the lateral distance (x-axis) and as a function of the angle of incidence. The incident beam impinges the layers at $z = z_a$, $x = 0$.

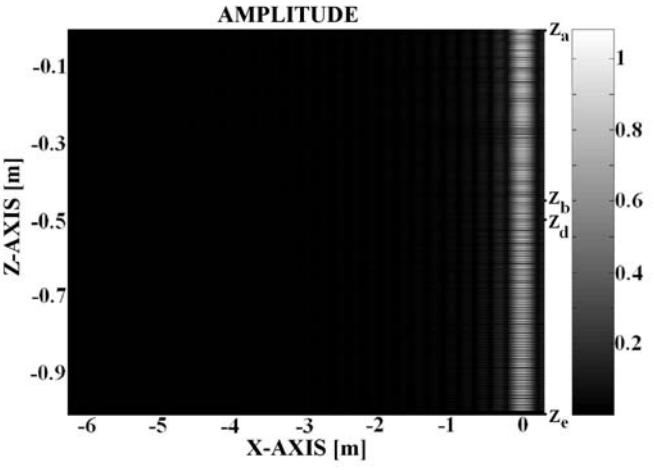

Figure 5. Total sound field inside the layers for angle of incidence 0°. This situation corresponds with classical echo sounding. The transition zone has no influence on the reflected beam.

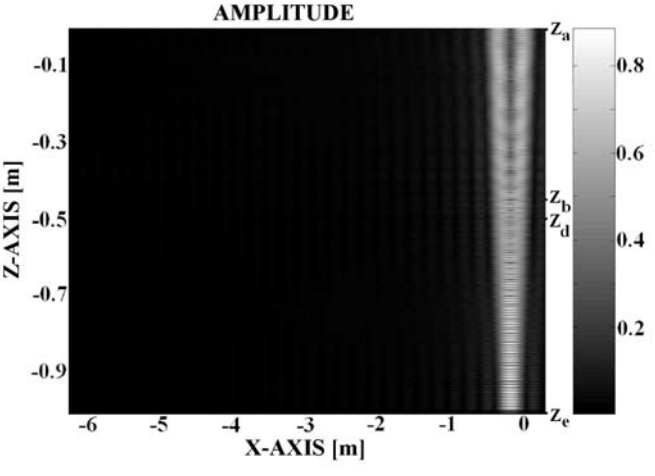

Figure 6. Total sound field inside the layers for angle of incidence 7.36°.

cur. It is seen in Figure 3 that, at 38.07°, an amplitude peak occurs for very low inhomogeneity. Hence, a very strong beam shift can be expected there. Furthermore, all other peaks for relatively low inhomogeneities are roughly situated in between 20° and 50°. It can therefore be expected that strong beam shifts will occur within that interval of incidence angles and that the strongest shift will appear at 38.07°.

5. Numerical results for incident bounded beams

It is worthwhile to present the total displacement field inside the rheological system in order to visualize how an incident bounded beam propagates and scatters through the different layers. We know that each incident inhomogeneous wave generates the acoustical potentials (31)–(40). If we take into account (31)–(40) and (43), then the displacement fields can be obtained. They are listed in the appendix (A25)–(A29). A continuous Gaussian beam of frequency 150 kHz and width 0.3 m, decomposed into plane waves using the Fourier decomposition, is impinging at the spot ($z = z_a$, $x = 0$). This is schematically visualized in Figure 1. The thereby generated normalized amplitude of the particle displacements along $z = z_a$ are depicted in Figure 4 as a function of the angle of incidence. Hence, the incident beam can be noticed at $x = 0$ and also the reflected sound is visible. Furthermore, it is noticed that the reflected 'beam' undergoes a sweep to larger distances and then back to smaller distances as the angle of incidence grows. This sweep exceedingly occurs in the interval between 20° and 50° and is strongest at 38.07° as was predicted in the previous paragraph. The phenomenon that causes this sweep is explained below, where the physical appearance of the bounded beam inside the layers is depicted. In Figures 5–10, the normalized amplitude of the particle displacements is depicted inside the layers and for angles of incidence corresponding to some remarkable spots in Figure 4. It is seen from Figure 5 that for

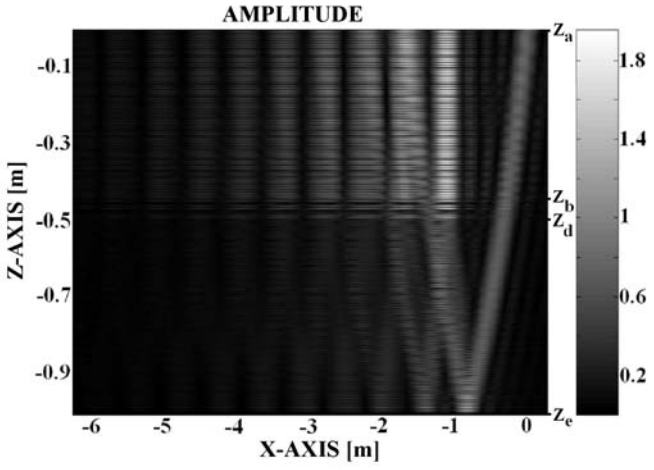

Figure 7. Total sound field inside the layers for angle of incidence 27.93°. It is clear that, contrary to Figure 5, the transition zone influences the reflected beam.

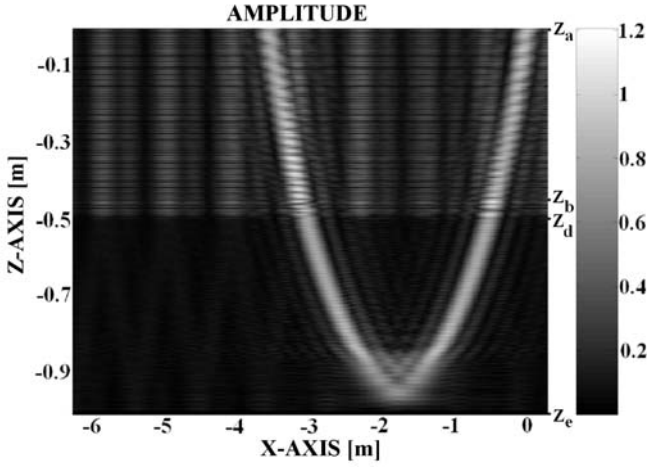

Figure 8. Total sound field inside the layers for angle of incidence 38.07°. This corresponds with the maximum sweep in Figure 4.

normal incidence, there is complete transmission through the transition layer. This is the reason why in echo sounding the transition layer is not detectable. From Figure 6 and Figure 7, it is seen that at more or less randomly chosen angles 7.36° respectively 27.93°, part of the sound is transmitted through the transition layer, while part is reflected. This shows that, even though there is no abrupt change but a strong continuous change in physical parameters, contrary to normally incident sound, obliquely incident sound is susceptible to the presence of the transition zone. There is however an angle of 38.07° at which the transition layer let incident sound pass completely. It is at this angle that a large beam sweep (or shift) is visible in Figure 4. The sweep happens because the bounded beam propagates over a large distance up to the underground, without being affected by the transition layer that crosses its path. For larger angles, incident sound gets reflected (see Figure 9) again in the transition layer. Furthermore, there is an angle of 55.53° at which the incident sound is perfectly reflected from the transition layer.

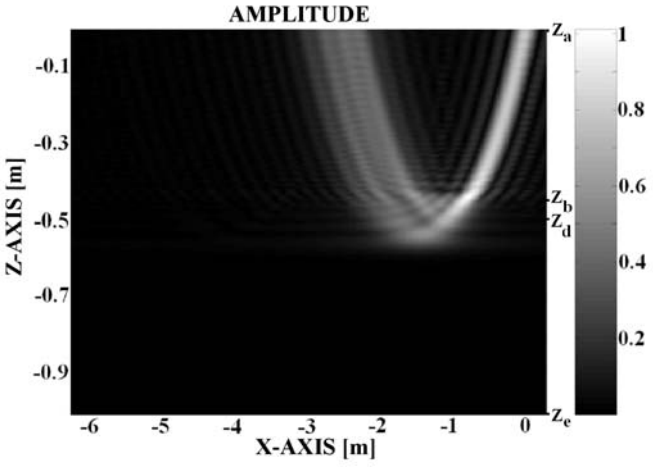

Figure 9. Total sound field inside the layers for angle of incidence 48.04°. There is no penetration into the non-navigable mud.

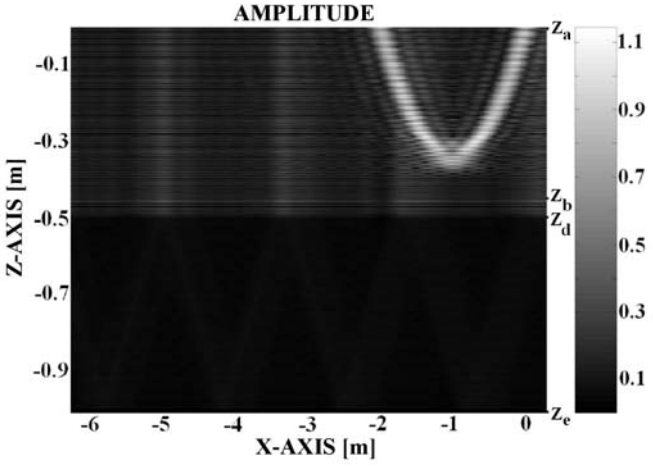

Figure 10. Total sound field inside the layers for angle of incidence 55.53°.

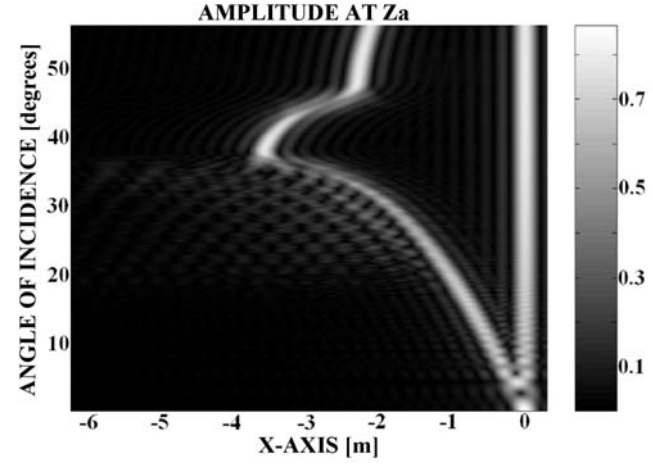

Figure 11. This figure is equal to Figure 4, except that here $z_b = -0.55$ m and $z_d = -0.6$ m, which means that the transition layer is 10 cm lower. The difference is noticeable in the reflected beam pattern and can be used to measure the nautical depth in harbors.

In the shipping and the dredging industry, it is important to find out where exactly the transition zone is situated in

order to determine the depth of the nautical bottom. Even though the physical parameters that are incorporated here do not perfectly correspond with the parameters of physical mud, it is interesting to show that the position of the transition zone influences the reflected beam profile for oblique incidence. Therefore we have repeated the calculation of Figure 4 in Figure 11, except for the only difference that the transition zone is now 10 cm deeper, i.e. $z_b = -0.55\,\mathrm{m}$ and $z_d = -0.60\,\mathrm{m}$.

Comparison of Figure 11 with Figure 4 shows that the reflected beam profile is indeed influenced by the depth of the transition zone, especially in the practicable range of small angles of incidence. The study of the reflected beam profile is hence a promising technique for determination of the nautical bottom. Further details are beyond the scope of this paper.

6. Concluding remarks

Contrary to existing models [42, 43] for 'discrete layers of homogeneous sediment material', a model is developed that is susceptible to simulate the interaction of sound with a liquid showing Bingham features (like mud), where layers of very fine sediment are involved possessing 'continuously varying material parameters', situated in between an ideal liquid and a hard solid. It is shown that the reflection coefficient for incident inhomogeneous waves shows peaks exceeding unity which are also present in earlier studies on discontinuously layered materials such as coated metal plates swamped in water. A qualitative study of these peaks has revealed strong beam displacements at certain angles. This was numerically confirmed by studying the interaction of bounded beams with the rheological system using the Fourier decomposition. This work shows that strong varying physical properties inside a continuously layered system may have serious consequences on impinging sound, such as total reflection or total transmission. Furthermore it is shown that the reflected beam profile for oblique incidence is influenced by the nautical depth. This may have important applications in the shipping and dredging industry.

Appendix

The different elements of the continuity matrix given in (47) are obtained and given in (A1)–(A7)

$$c1 = \begin{bmatrix} -2\mu_w k_{inc,x} k_{inc,z} & P_{md,ab,0} & P_{wd,ab,0} & \\ \mathrm{i}k_{inc,z} & P_{md,ab,1} & P_{wd,ab,1} & \cdots \\ \rho_w\omega^2 - 2\mu_w k_{inc,x}^2 & P_{md,ab,2} & P_{wd,ab,2} & \\ \mu_{ab}(z_a)[-k_{inc,x}^2 + g_{s,ab}(z_a)] & P_{ws,ab,0} & & \\ \cdots \quad \mathrm{i}k_{inc,x} & P_{ws,ab,1} & & \\ -2\mu_{ab}(z_a)k_{inc,x}\sqrt{\tilde{k}_{s,ab}} & P_{ws,ab,2} & & \end{bmatrix} \quad \text{(A1)}$$

$$c2 = \begin{bmatrix} 0 & 0 & 0 & \\ 0 & \mathrm{Ary}_0\big(\gamma_{d,ab}(z_b)\big) & \mathrm{Ary}_2\big(\gamma_{d,ab}(z_b)\big) & \cdots \\ 0 & 0 & 0 & \\ 0 & -\frac{\bar{p}_{d,ab}\,\mathrm{Ary}_1\left(\gamma_{d,ab}(z_b)\right)}{(-\bar{p}_{d,ab})^{2/3}} & -\frac{\bar{p}_{d,ab}\,\mathrm{Ary}_3\left(\gamma_{d,ab}(z_b)\right)}{(-\bar{p}_{d,ab})^{2/3}} & \\ \exp\left(\mathrm{i}\sqrt{\tilde{k}_{s,ab}}(z_b - z_a)\right) & 1 & & \\ \cdots \quad 0 & 0 & & \\ \mathrm{i}\sqrt{\tilde{k}_{s,ab}}\exp\left(\mathrm{i}\sqrt{\tilde{k}_{s,ab}}(z_b - z_a)\right) & -\mathrm{i}\sqrt{\tilde{k}_{s,ab}} & & \\ 0 & 0 & & \end{bmatrix} \quad \text{(A2)}$$

$$c3 = \begin{bmatrix} 0 & 0 & & \\ -\mathrm{Ary}_0\big(\gamma_{d,bd}(z_b)\big) & -\mathrm{Ary}_2\big(\gamma_{d,bd}(z_b)\big) & & \\ 0 & 0 & \cdots & \\ \frac{\bar{p}_{d,bd}\,\mathrm{Ary}_1\left(\gamma_{d,bd}(z_b)\right)}{(-\bar{p}_{d,bd})^{2/3}} & \frac{\bar{p}_{d,ab}\,\mathrm{Ary}_3\left(\gamma_{d,bd}(z_b)\right)}{(-\bar{p}_{d,bd})^{2/3}} & & \\ -\mathrm{Ary}_0\big(\gamma_{s,bd}(z_b)\big) & -\mathrm{Ary}_2\big(\gamma_{s,bd}(z_b)\big) & & \\ 0 & 0 & & \\ \cdots \quad \frac{\bar{p}_{s,bd}\,\mathrm{Ary}_1\left(\gamma_{s,bd}(z_b)\right)}{(-\bar{p}_{s,bd})^{2/3}} & \frac{p_{s,bd}\,\mathrm{Ary}_3\left(\gamma_{s,bd}(z_b)\right)}{(-\bar{p}_{s,bd})^{2/3}} & & \\ 0 & 0 & & \end{bmatrix} \quad \text{(A3)}$$

$$c4 = \begin{bmatrix} 0 & 0 & & \\ \mathrm{Ary}_0\big(\gamma_{d,bd}(z_d)\big) & \mathrm{Ary}_2\big(\gamma_{d,bd}(z_d)\big) & & \\ 0 & 0 & \cdots & \\ \frac{\bar{p}_{d,bd}\,\mathrm{Ary}_1\left(\gamma_{d,bd}(z_d)\right)}{(-\bar{p}_{d,bd})^{2/3}} & -\frac{\bar{p}_{d,ab}\,\mathrm{Ary}_3\left(\gamma_{d,bd}(z_d)\right)}{(-\bar{p}_{d,bd})^{2/3}} & & \\ \mathrm{Ary}_0\big(\gamma_{s,bd}(z_d)\big) & \mathrm{Ary}_2\big(\gamma_{s,bd}(z_d)\big) & & \\ 0 & 0 & & \\ \cdots \quad -\frac{\bar{p}_{s,bd}\,\mathrm{Ary}_1\left(\gamma_{s,bd}(z_d)\right)}{(-\bar{p}_{s,bd})^{2/3}} & -\frac{\bar{p}_{s,bd}\,\mathrm{Ary}_3\left(\gamma_{s,bd}(z_d)\right)}{(-\bar{p}_{s,bd})^{2/3}} & & \\ 0 & 0 & & \end{bmatrix} \quad \text{(A4)}$$

$$c5 = \begin{bmatrix} 0 & 0 & & \\ -\mathrm{Ary}_0\big(\gamma_{d,de}(z_d)\big) & -\mathrm{Ary}_2\big(\gamma_{d,de}(z_d)\big) & & \\ 0 & 0 & \cdots & \\ \frac{\bar{p}_{d,de}\,\mathrm{Ary}_1\left(\gamma_{d,de}(z_d)\right)}{(-\bar{p}_{d,de})^{2/3}} & \frac{\bar{p}_{d,de}\,\mathrm{Ary}_3\left(\gamma_{d,de}(z_d)\right)}{(-\bar{p}_{d,de})^{2/3}} & & \\ -1 & -\exp\big(-\mathrm{i}\sqrt{\tilde{k}_{s,de}}(z_d - z_e)\big) & & \\ 0 & 0 & & \\ -\mathrm{i}\sqrt{\tilde{k}_{s,de}} & \mathrm{i}\sqrt{\tilde{k}_{s,de}}\exp\big(-\mathrm{i}\sqrt{\tilde{k}_{s,de}}(z_d - z_e)\big) & & \\ 0 & 0 & & \end{bmatrix} \quad \text{(A5)}$$

$$c6 = \begin{bmatrix} \mathrm{i}k_{inc,x}\mathrm{Ary}_0\big(\gamma_{d,de}(z_e)\big) & \mathrm{i}k_{inc,x}\mathrm{Ary}_2\big(\gamma_{d,de}(z_e)\big) & & \\ -\frac{\bar{p}_{d,de}\,\mathrm{Ary}_1\left(\gamma_{d,de}(z_e)\right)}{(-\bar{p}_{d,de})^{2/3}} & -\frac{\bar{p}_{d,de}\,\mathrm{Ary}_3\left(\gamma_{d,de}(z_e)\right)}{(-\bar{p}_{d,de})^{2/3}} & & \\ P_{md,de,13} & P_{wd,de,13} & & \\ P_{md,de,14} & P_{wd,de,14} & & \\ -\mathrm{i}\sqrt{\tilde{k}_{s,de}}\exp\left(\mathrm{i}\sqrt{k_{s,de}}(z_e - z_d)\right) & \mathrm{i}\sqrt{\tilde{k}_{s,de}} & & \\ \mathrm{i}k_{inc,x}\exp\left(\mathrm{i}\sqrt{\tilde{k}_{s,de}}(z_e - z_d)\right) & \mathrm{i}k_{inc,x} & & \\ P_{ms,de,13} & P_{ws,de,13} & & \\ P_{ms,de,14} & P_{ws,de,14} & & \end{bmatrix} \quad \text{(A6)}$$

$$c7 = \begin{bmatrix} -\mathrm{i}k_{inc,x} & \mathrm{i}k^{s}_{u,z} \\ -\mathrm{i}k^{d}_{u,z} & -\mathrm{i}k_{inc,x} \\ 2\mu_u k_{inc,x} k^{d}_{u,z} & \mu_u (k^{2}_{inc,x} - \mu_u g_{s,u}) \\ \lambda_u k^{2}_{inc,x} + (\lambda_u + 2\mu_u) g_{d,u} & 2\mu_u k_{inc,x} k^{s}_{u,z} \end{bmatrix} \quad \text{(A7)}$$

with, in (A1)–(A7):

$$P_{md,ab,0} = -2\mathrm{i}\mu_{ab}(z_a) k_{inc,x} \frac{\tilde{p}_{d,ab} \mathrm{Ary}_1\big(\gamma_{d,ab}(z_a)\big)}{(-\tilde{p}_{d,ab})^{2/3}} \quad \text{(A8)}$$

$$P_{wd,ab,0} = -2\mathrm{i}\mu_{ab}(z_a) k_{inc,x} \frac{\tilde{p}_{d,ab} \mathrm{Ary}_3\big(\gamma_{d,ab}(z_a)\big)}{(-\tilde{p}_{d,ab})^{2/3}} \quad \text{(A9)}$$

$$P_{ws,ab,0} = \mu_{ab}(z_a)\big[-k^{2}_{inc,x} + g_{s,ab}(z_a)\big] \cdot \exp\Big(-\mathrm{i}\sqrt{\tilde{k}_{s,ab}}(z_a - z_b)\Big) \quad \text{(A10)}$$

$$P_{md,ab,1} = -\frac{\tilde{p}_{d,ab}}{(-\tilde{p}_{d,ab})^{2/3}} \mathrm{Ary}_1\big(\gamma_{d,ab}(z_a)\big) \quad \text{(A11)}$$

$$P_{wd,ab,1} = -\frac{\tilde{p}_{d,ab}}{(-\tilde{p}_{d,ab})^{2/3}} \mathrm{Ary}_3\big(\gamma_{d,ab}(z_a)\big) \quad \text{(A12)}$$

$$P_{ws,ab,1} = \mathrm{i}k_{inc,x} \exp\Big(-\mathrm{i}\sqrt{\tilde{k}_{s,ab}}(z_a - z_b)\Big) \quad \text{(A13)}$$

$$P_{md,ab,2} = \Big[-\lambda_{ab}(z_a) k^{2}_{inc,x} - \big(\lambda_{ab}(z_a) + 2\mu_{ab}(z_a)\big) g_{d,ab}(z_a)\Big] \mathrm{Ary}_0\big(\gamma_{d,ab}(z_a)\big) \quad \text{(A14)}$$

$$P_{wd,ab,2} = \Big[-\lambda_{ab}(z_a) k^{2}_{inc,x} - \big(\lambda_{ab}(z_a) + 2\mu_{ab}(z_a)\big) g_{d,ab}(z_a)\Big] \mathrm{Ary}_2\big(\gamma_{d,ab}(z_a)\big) \quad \text{(A15)}$$

$$P_{ws,ab,2} = 2\mu_{ab}(z_a) k_{inc,x} \sqrt{\tilde{k}_{s,ab}} \cdot \exp\Big(-\mathrm{i}\sqrt{\tilde{k}_{s,ab}}(z_a - z_b)\Big) \quad \text{(A16)}$$

$$P_{md,de,13} = -2\mathrm{i}\mu_{de}(z_e) k_{inc,x} \frac{\tilde{p}_{d,de}}{(-\tilde{p}_{d,de})^{2/3}} \cdot \mathrm{Ary}_1\big(\gamma_{d,de}(z_e)\big) \quad \text{(A17)}$$

$$P_{wd,de,13} = -2\mathrm{i}\mu_{de}(z_e) k_{inc,x} \frac{\tilde{p}_{d,de}}{(-\tilde{p}_{d,de})^{2/3}} \cdot \mathrm{Ary}_3\big(\gamma_{d,de}(z_e)\big) \quad \text{(A18)}$$

$$P_{ms,de,13} = \mu_{de}(z_e)\big[-k^{2}_{inc,x} + g_{s,de}(z_e)\big] \cdot \exp\Big(\mathrm{i}\sqrt{\tilde{k}_{s,de}}(z_e - z_d)\Big) \quad \text{(A19)}$$

$$P_{ws,de,13} = \mu_{de}(z_e)\big[-k^{2}_{inc,x} + g_{s,de}(z_e)\big] \quad \text{(A20)}$$

$$P_{md,de,14} = -\Big[\big(\lambda_{de}(z_e) + 2\mu_{de}(z_e)\big) g_{d,de}(z_e) + \lambda_{de}(z_e) k^{2}_{inc,x}\Big] \mathrm{Ary}_0\big(\gamma_{d,de}(z_e)\big) \quad \text{(A21)}$$

$$P_{wd,de,14} = -\Big[\big(\lambda_{de}(z_e) + 2\mu_{de}(z_e)\big) g_{d,de}(z_e) + \lambda_{de}(z_e) k^{2}_{inc,x}\Big] \mathrm{Ary}_2\big(\gamma_{d,de}(z_e)\big) \quad \text{(A22)}$$

$$P_{ms,de,14} = -2\mu_{de}(z_e) k_{inc,x} \sqrt{\tilde{k}_{s,de}} \cdot \exp\Big(\mathrm{i}\sqrt{\tilde{k}_{s,de}}(z_e - z_d)\Big) \quad \text{(A23)}$$

$$P_{ws,de,14} = 2\mu_{de}(z_e) k_{inc,x} \sqrt{\tilde{k}_{s,de}}. \quad \text{(A24)}$$

The particle displacement fields within the different layers of the rheological system are given as:

$$\begin{aligned} \boldsymbol{u}_w = {} & \mathrm{i}k_{inc,x}\Big[Q \exp\big(-\mathrm{i}k_{inc,z}(z - z_a)\big) + A \exp\big(\mathrm{i}k_{inc,z}(z - z_0)\big)\Big] \exp\big(\mathrm{i}k_{inc,x} x\big) \boldsymbol{e}_x \\ & + \mathrm{i}k_{inc,z}\Big[-Q \exp\big(-\mathrm{i}k_{inc,z}(z - z_a)\big) + A \exp\big(\mathrm{i}k_{inc,z}(z - z_0)\big)\Big] \exp\big(\mathrm{i}k_{inc,x} x\big) \boldsymbol{e}_z \end{aligned} \quad \text{(A25)}$$

$$\begin{aligned} \boldsymbol{u}_{ab} = {} & \mathrm{i}k_{inc,x}\Big(C_{md,ab}\mathrm{Ary}_0(\gamma_{d,ab}) + C_{wd,ab}\mathrm{Ary}_2(\gamma_{d,ab})\Big) \cdot \exp(\mathrm{i}k_{inc,x} x) \boldsymbol{e}_x \\ & - \mathrm{i}\sqrt{\tilde{k}_{s,ab}}\Big[C_{ms,ab} \exp\Big(\mathrm{i}\sqrt{\tilde{k}_{s,ab}}(z - z_a)\Big) - C_{ws,ab} \exp\Big(-\mathrm{i}\sqrt{\tilde{k}_{s,ab}}(z - z_b)\Big)\Big] \cdot \exp\big(\mathrm{i}k_{inc,x} x\big)\Big] \boldsymbol{e}_x \\ & - \frac{\tilde{p}_{d,ab}}{(-\tilde{p}_{d,ab})^{2/3}} \exp\big(\mathrm{i}k_{inc,x} x\big) \cdot \big(C_{md,ab}\mathrm{Ary}_1(\gamma_{d,ab}) + C_{wd,ab}\mathrm{Ary}_3(\gamma_{d,ab})\big) \boldsymbol{e}_z \\ & + \mathrm{i}k_{inc,x} \exp\big(\mathrm{i}k_{inc,x} x\big) \cdot \Big[C_{ms,ab} \exp\Big(\mathrm{i}\sqrt{\tilde{k}_{s,ab}}(z - z_a)\Big) + C_{ws,ab} \exp\Big(-\mathrm{i}\sqrt{\tilde{k}_{s,ab}}(z - z_b)\Big)\Big] \boldsymbol{e}_z \end{aligned} \quad \text{(A26)}$$

$$\begin{aligned} \boldsymbol{u}_{bd} = {} & \mathrm{i}k_{inc,x}\Big(C_{md,bd}\mathrm{Ary}_0(\gamma_{d,bd}) + C_{wd,bd}\mathrm{Ary}_2(\gamma_{d,bd})\Big) \cdot \exp(\mathrm{i}k_{inc,x} x) \boldsymbol{e}_x \\ & + \frac{\tilde{p}_{s,bd}}{(-\tilde{p}_{s,bd})^{2/3}} \exp\big(\mathrm{i}k_{inc,x} x\big) \cdot \big(C_{ms,bd}\mathrm{Ary}_1(\gamma_{s,bd}) + C_{ws,bd}\mathrm{Ary}_3(\gamma_{s,bd})\big) \boldsymbol{e}_x \\ & - \frac{\tilde{p}_{d,bd}}{(-\tilde{p}_{d,bd})^{2/3}} \exp\big(\mathrm{i}k_{inc,x} x\big) \end{aligned}$$

$$\cdot \left(C_{md,bd}\mathrm{Ary}_1(\gamma_{d,bd}) + C_{wd,bd}\mathrm{Ary}_3(\gamma_{d,bd})\right)\boldsymbol{e}_z$$
$$+ \mathrm{i}k_{inc,x}\exp\left(\mathrm{i}k_{inc,x}x\right) \qquad \text{(A27)}$$
$$\cdot \left(C_{ms,bd}\mathrm{Ary}_0(\gamma_{s,bd}) + C_{ws,bd}\mathrm{Ary}_2(\gamma_{s,bd})\right)\boldsymbol{e}_z$$

$$\begin{aligned}\boldsymbol{u}_{de} \;=\; & \mathrm{i}k_{inc,x}\left(C_{md,de}\mathrm{Ary}_0(\gamma_{d,de}) + C_{wd,de}\mathrm{Ary}_2(\gamma_{d,de})\right)\\ & \cdot \exp(\mathrm{i}k_{inc,x}x)\boldsymbol{e}_x\\ & - \mathrm{i}\sqrt{\tilde{k}_{s,de}}\left[C_{ms,de}\exp\left(\mathrm{i}\sqrt{\tilde{k}_{s,de}}(z-z_d)\right)\right.\\ & \left. - C_{ws,de}\exp\left(-\mathrm{i}\sqrt{\tilde{k}_{s,de}}(z-z_e)\right)\right]\\ & \cdot \exp\left(\mathrm{i}k_{inc,x}x\right)\boldsymbol{e}_x\\ & - \frac{\tilde{p}_{d,de}}{(-\tilde{p}_{d,de})^{2/3}}\exp\left(\mathrm{i}k_{inc,x}x\right)\\ & \cdot \left(C_{md,de}\mathrm{Ary}_1(\gamma_{d,de}) + C_{wd,de}\mathrm{Ary}_3(\gamma_{d,de})\right)\boldsymbol{e}_z\\ & + \mathrm{i}k_{inc,x}\exp\left(\mathrm{i}k_{inc,x}x\right) \qquad \text{(A28)}\\ & \cdot \left[C_{ms,de}\exp\left(\mathrm{i}\sqrt{\tilde{k}_{s,de}}(z-z_d)\right)\right.\\ & \left. + C_{ws,de}\exp\left(-\mathrm{i}\sqrt{\tilde{k}_{s,de}}(z-z_e)\right)\right]\boldsymbol{e}_z\end{aligned}$$

$$\begin{aligned}\boldsymbol{u}_u \;=\; & \left[\mathrm{i}k_{inc,x}D\exp\left(\mathrm{i}k^d_{u,z}(z-z_e)\right)\right.\\ & \left. - \mathrm{i}k^s_{u,z}S\exp\left(\mathrm{i}k^s_{u,z}(z-z_e)\right)\right]\exp\left(\mathrm{i}k_{inc,x}x\right)\boldsymbol{e}_x\\ & + \left[\mathrm{i}k^d_{u,z}D\exp\left(\mathrm{i}k^d_{u,z}(z-z_e)\right)\right. \qquad \text{(A29)}\\ & \left. + \mathrm{i}k_{inc,x}S\exp\left(\mathrm{i}k^s_{u,z}(z-z_e)\right)\right]\exp\left(\mathrm{i}k_{inc,x}x\right)\boldsymbol{e}_z.\end{aligned}$$

Acknowledgement

This research is sponsored by 'The Flemish Institute for the Encouragement of the Scientific and Technological Research in Industry (I.W.T.)'. The authors also wish to thank

- Haecon Harbour & Engineering Consultants, Drongen, Belgium;
- Verhaert Space Instruments & Applied Technologies, Kruibeke, Belgium;
- Department of Chemical Engineering Techniques, Katholieke Universiteit Leuven, Heverlee, Belgium

for fruitful discussions and for sharing their enthusiasm with us.

References

[1] H. Okamura, K. Maekawa, K. Ozawa: High performance concrete (in Japanese). Gihou-Dou Pub., 1993.

[2] F. DeLarrard, C. Hu, T. Sedran, J. C. Sitzkar, M. Joly, F. Claux, F. Derkx: A new rheometer for soft-to-fluid fresh concrete. ACI Materials Journal **94** (May-June, 1997) 234–243.

[3] M. Dragoni, M. Bonafede, E. Boschi: Downslope flow models of Bingham liquid: implications for lava flows. J. Vulcanol. Geotherm. Res. **30** (1986) 305–325.

[4] T. K. P. Gregg, S. E. H. Sakimoto: Inside the black box: velocity distributions and flow rates in lava channels from laboratory, analytic and computational fluid dynamics methods. Lunar and Planetary science **XXIX** (1998) 1499. Proceedings of 'Lunar and Planetary Science Conference', Houston, Texas.

[5] E. Brown: What is bottom? Soundings, Lighthouse journal of the Canadian Hydrographic Association (CHA) edition 60 (2002).

[6] W. Dasch, R. Wurpts: Isoviscs as useful parameters for describing sedimentation. Terra et Aqua International Journal on Public Works, Ports and Waterways Developments **82** (2001).

[7] R. Wurpts: The question of definition of the nautical depth in fluid mud by the aid of rheological properties. Proceedings of the 15th World Dredging Congress 'Dredging into the 21st century', 1998, 457.

[8] J.-y. Xu, J.-z. Yuan: Study on the fluid mud in the Yangtze estuary. Journal of Sediment Research **3** (2001).

[9] S. Wartel: Mud layers and cyclic sedimentation patterns in the estuary of the Schelde (Belgium). Proceedings of IGCP, Réunion Internationale PICG274, Evolution côtiere au Quaternaire, Dakar, 46-47, 1993.

[10] S. Bentley, H. H. Roberts: Fluid mud: Worldwide importance in rapid coastal dispersal of fine-grained sediments. AAPG Annual Meeting 2002: Our Heritage-Key to Global Discovery, Houston, March 10-13, 2002, paper 43322.

[11] P. T. Harris, R. Coleman: Estimating global shelf sediment mobility due to swell waves. Marine Geology **150** (1998) 171–177.

[12] The Malay Mail: Mud study to trace evolution, sediment from sea-depths reveal secrets of earth's changes. July 23, 1993.

[13] H. Singh, J. Adams, D. Mindell, B. P. Foley: Imaging underwater for archaeology. Journal of Field Archaeology **27** (2000) 319–328.

[14] D. A. Mindell, B. Bingham: A high-frequency, narrow-beam sub-bottom profiler for archaeological applications. Proceedings of IEEE Oceans 2001 Conference, 2001.

[15] J.-D. Stanley, F. Goddio, G. Schnepp: Nile flooding sank two ancient cities. Nature **412** (2001) 293–294.

[16] D. Verschuren, K. R. Laird, B. F. Cumming: Rainfall and drought in equatorial east Africa during the past 1,100 years. Nature **403** (2000) 410–414.

[17] R. G. Rothwell, J. Thomson, G. Köhler: Low-sea-level emplacement of a very large Late Pleistocene 'megaturbidite' in the western Mediterranean Sea. Nature **392** (1998) 377–380.

[18] J. Li, Y. Renardy: Shear-induced rupturing of a viscous drop in a Bingham liquid. J. Non-Newtonian Fluid Mechanics **95** (2000) 235–251.

[19] T. Byerly: Building a better bridge. Government Technology, November 1998.

[20] Atema, Jelle, D. F. Leavitt, D. E. Barshaw, M. C. Cuomo: Effects of drilling muds on behavior of the American lobster, Homarus americanus, in water column and substrate exposures. Can. J. Fish. Aquat. Sci. **39** (1982) (ERL,GB X298), 675–689.

[21] H. De Vlieger: Navitracker – a towed density probe for continous measurement of sediment density. Terra et Aqua, International Journal on Public Works, Ports and Waterways development (1987).

[22] J. V. Gardner, P. Dartnell, H. Gibbons, D. MacMillan: Exposing the sea floor: High-resolution multibeam mapping along the U.S. Pacific coast. U.S. Geological Survey Fact Sheet 013-00, 2000.

[23] R. A. Stephen: Bottom penetration at subcritical grazing angles by scattering. J. Acoust. Soc. Am. **99** (1996) 2475–2500.

[24] J. R. Banic, A. G. Cunningham: Airborne laser bathymetry: A tool for the next millennium. EEZ Technology **3** (1998) 75–80.

[25] F. A. Boyle, N. P. Chotiros: A model for acoustic backscatter from muddy sediments. J. Acoust. Soc. Am. **98** (1995) 525–530.

[26] K. B. Briggs, M. D. Richardson, D. R. Jackson: High-frequency bottom backscattering: Volume scattering from gassy mud. J. Acoust. Soc. Am. **96** (1994) 3218.

[27] P. D. M.Spelt, M. A. Norato, A. S. Sangani, L. L. Tavlarides, M. S. Greenwood: Attenuation of sound in concentrated suspensions: theory and experiments. Journal of Fluid Mechanics **430** (2001) 51–86.

[28] W. R. Bryant, M. D. Richardson: Permeability and porosity of clayey sediments in seismo-acoustics. J. Acoust. Soc. Am. **92** (1992) 2308.

[29] L. M. Brekhovskikh, O. A. Godin: Acoustics of layered media I. Springer Series on Wave Phenomena, 1998.

[30] B. Poirée: Complex harmonic plane waves. – In: Physical Acoustics. O. Leroy, M. A. Breazeale (eds.). Plenum Press, New York, 1991.

[31] J. P. Charlier, F. Crowet: Wave equations in linear viscoelastic materials. J. Acoust. Soc. Am. **79** (1986) 895–900.

[32] M. Deschamps, C. L. Cheng: Liquid-thermoviscoelastic solids interface. Ultrasonics **27** (1989) 308–313.

[33] M. J. Buckingham: Theory of compressional and shear waves in fluidlike marine sediments. J. Acoust. Soc. Am. **103** (1998) 288–299.

[34] E. L. Hamilton: Attenuation of shear waves in marine sediments. J. Acoust. Soc. Am. **60** (1976) 334–338.

[35] E. L. Hamilton: Sound attenuation as a function of depth in the sea floor. J. Acoust. Soc. Am. **59** (1976) 528–535.

[36] K. Van Den Abeele: Alternative fundamental theoretical descriptions for acousto-optic and acoustic investigation of pulsed and profiled ultrasound in view of nondestructive testing of layered structures. PhD Thesis, Department of Sciences, KUL Campus Kortrijk, 1992.

[37] K. F. Herzfeld, T. A. Litovitz: Absorption and dispersion of ultrasound waves. Academic, New York, 1959.

[38] W. M. Madigosky, R. W. Warfield: The magnitude of ultrasonic volume viscosity. Acustica **55** (1984) 123–127.

[39] M. Abramowitz, I. A. Stegun (eds.): Handbook of mathematical functions. Dover publications, 1972.

[40] M. Deschamps, P. Chevée: Reflection and refraction of a heterogeneous plane wave by a solid layer. Wave Motion **15** (1992) 61–75.

[41] J. M. Claeys, O. Leroy: Reflection and transmission of bounded sound beams on half-spaces and through plates. J. Acoust. Soc. Am. **72** (1982) 585–590.

[42] H. Schmidt, F. B. Jensen: A full wave solution for propagation in multilayered viscoelestic media with application to Gaussian beam reflection at fluid-solid interfaces. J. Acoust. Soc. Am. **77** (1985) 813–825.

[43] F. B. Jensen, H. Schmidt: Subcritical penetration of narrow Gaussian beams into sediments. J. Acoust. Soc. Am. **82** (1987) 574–579.